From Small Fullerenes to the Graphene Limit: A Harmonic Force-Field Method for Fullerenes and a Comparison to Density Functional Calculations for Goldberg–Coxeter Fullerenes up to C_{980}

Lukas N. Wirz,[a] Ralf Tonner,[b] Andreas Hermann,[c] Rebecca Sure,[d] and Peter Schwerdtfeger*[e,f]

We introduce a simple but computationally very efficient harmonic force field, which works for all fullerene structures and includes bond stretching, bending, and torsional motions as implemented into our open-source code *Fullerene*. This gives accurate geometries and reasonably accurate vibrational frequencies with root mean square deviations of up to 0.05 Å for bond distances and 45.5 cm^{-1} for vibrational frequencies compared with more elaborate density functional calculations. The structures obtained were used for density functional calculations of Goldberg–Coxeter fullerenes up to C_{980}. This gives a rather large range of fullerenes making it possible to extrapolate to the graphene limit. Periodic boundary condition calculations using density functional theory (DFT) within the projector augmented wave method gave an energy difference between −8.6 and −8.8 kcal/mol at various levels of DFT for the reaction C_{60}→graphene (per carbon atom) in excellent agreement with the linear extrapolation to the graphene limit (−8.6 kcal/mol at the Perdew–Burke–Ernzerhof level of theory).

DOI: 10.1002/jcc.23894

Introduction

Fullerenes are hollow polyhedral carbon structures consisting of 12 pentagons and F_6 hexagons with $F_6 \geq 0$ and $F_6 \neq 1$.[1–4] Schleyer and coworkers pointed out that both C_{20}-I_h and C_{60}-I_h are not spherically π aromatic[5] but spherically π antiaromatic,[6] which for C_{60} explains the large heat of formation (for a more detailed discussion of fullerene aromaticity see Ref. [7]). They concluded that against common belief, fullerenes are not highly stable molecules,[6] showing no "magic" stability for C_{60} compared with other fullerenes (and graphene).

As the pentagons can be distributed in many different ways on a 2D surface (of genus zero),[3] the number of isomers grows rapidly with increasing number of carbon atoms N, that is, Thurston established a $\mathcal{O}(N^9)$ polynomial growth for the number of isomers with vertex number N.[8] These isomers come in many different shapes and symmetries,[9] and it is clear that a fast algorithm is required to determine accurate molecular shapes, which can further be refined by a more rigorous quantum theoretical treatment. Such an algorithm should give the right bond distances and angles for the 12 pentagons and F_6 hexagons, and the 3D structure should have the right symmetry, shape, and Gaussian curvature (which is predominantly positive but may be slightly negative locally in fullerenes).[9]

The fullerene graph $G=(V,E)$ with vertices $v_i \in V(i=1,\ldots,N)$ and edges $e_j \in E(j=1,\ldots,3N/2)$ contains all the information required to construct a structural carbon framework. A compact short-hand notation for fullerene graphs is given by the Fowler–Manolopoulos face-spiral algorithm, which, starting from a selected face, goes through all faces of the fullerene exactly once, that is, it is identical to a Hamilton spiral path for the dual of the fullerene. Only the locations of the pentagons need to be listed, and if the spiral gets stuck in a *cul-de-sac*, one can define jumps to remedy the situation. This leads to a generalized spiral algorithm which uniquely defines the fullerene graph. Conversely, from the general face spiral, one obtains the graph G (and its vertex adjacency matrix A_{kl}), which can be used to embed the graph on an appropriate 2D surface to obtain an

[a] *L. N. Wirz*
Centre for Theoretical Chemistry and Physics, The New Zealand Institute for Advanced Study, Massey University Auckland, Private Bag 102904, 0745, Auckland, New Zealand
[b] *R. Tonner*
Fachbereich Chemie, Philipps-Universität Marburg, Hans-Meerwein-Str., D-35032, Marburg, Germany
[c] *A. Hermann*
Centre for Science at Extreme Conditions and SUPA, School of Physics and Astronomy, The University of Edinburgh, Edinburgh, EH9 3FD, United Kingdom
[d] *R. Sure*
Mulliken Center for Theoretical Chemistry, University of Bonn, Beringstr. 4, 53115, Bonn, Germany
[e] *P. Schwerdtfeger*
Centre for Theoretical Chemistry and Physics, The New Zealand Institute for Advanced Study, Massey University Auckland, Private Bag 102904, 0745 Auckland, New Zealand
E-mail: p.a.schwerdtfeger@massey.ac.nz
[f] *P. Schwerdtfeger*
Fachbereich Chemie, Philipps-Universität Marburg, Hans-Meerwein-Str., D-35032 Marburg, Germany

Contract/grant sponsor: Alexander von Humboldt Foundation (Bonn) in terms of a Humboldt Research Award (P.S.).

initial 3D structure. Such 2D embedding algorithms are already available, for example, the Adjacency Matrix Eigenvector (AME) algorithm introduced by Fowler and Manolopoulos,[3,9,10] or the more recent combination of the Tutte embedding of the graph onto a 2D plane with subsequent projection onto the surface of a sphere, which was developed in our group.[9,11]

The next step is to refine the initial crude 3D geometry by a force-field optimization, which should lead to a structure close to the real (experimental) one. It is common for molecular force fields to distinguish between single and double bonds. This strategy, however, is not practical for fullerenes due to exponential growth of different Kekulé structures with increasing vertex number *N*. Force fields for fullerenes should therefore be designed avoiding the distinction between single and double bonds. The first force field tailored specifically to fullerenes was developed by Wu et al.[12] It was designed for C_{60}-I_h only using harmonic force field terms between two bond types: Bonds adjacent to two hexagons with a bond length of 1.54 Å, and bonds adjacent to a pentagon and a hexagon with a bond length of 1.41 Å. Angles are either part of a pentagon ($\theta_0 = \frac{3}{5}\pi$) or a hexagon ($\theta_0 = \frac{2}{3}\pi$).

A number of extensions and modifications to the Wu force field have been published since.[13–18] Except for the force field by Ceulemans et al.,[17] all others have been exclusively designed for C_{60}-I_h. Here, we introduce a harmonic force field applicable to all fullerenes as implemented into our program package *Fullerene*, and test the obtained structures for larger fullerenes (obtained from Goldberg–Coxeter transforms of C_{20}) against more accurate density functional theory (DFT) calculations. As an illustrative example, we use the DFT electronic energies to extrapolate to the graphene limit, and compare our results to periodic DFT calculations for graphene.[19,20] The force-field vibrational frequencies are also used to extrapolate to the zero-point energy limit of graphene.

Computational Methods

The initial fullerene structures were generated by the program Fullerene* through a face-spiral algorithm,[21] a Tutte embedding of the graph and subsequent mapping of the planar layout on a sphere followed by a geometry optimization using the general fullerene force field as introduced in the next chapter. We chose the most stable fullerene structures for each vertex number up to C_{60} (see Ref. [22] for details), plus some selected fullerenes up to C_{100}. As candidates for larger fullerenes beyond 100 vertices, we chose the Goldberg–Coxeter transforms[3,23,24] of C_{20}, that is, $GC_{k,l}[C_{20}\text{-}I_h] = C_N$ with $N = 20(k^2 + kl + l^2) \leq 980$. These icosahedral structures were taken as input for refined optimization using DFT. In a first step, the structures were optimized with the Perdew–Burke–Ernzerhof (PBE) functional[25] using the def2-TZVPP basis set for the fullerenes from C_{20} up to C_{60}, and the smaller def2-SVP basis set[26] for the larger fullerenes (from C_{60} onwards) within the Gaussian09 code.[27] Tight geometry convergence criteria and ultra-fine integration grids were applied and the symmetry of the structures was exploited. Starting from these structures, subsequent optimizations for the larger fullerenes were carried out with the Becke–Lee–Yang–Parr hybrid functional (B3LYP)[28,29] functional as implemented in Gaussian09 and Turbomole (for the optimized structures see Supplementary Information).[27,30] This was done to obtain a second value for the graphene limit. We only chose these two commonly applied functionals as some of the calculations for the larger fullerenes became very computer time intensive. All structures were treated as closed-shell singlet molecules, except for some of the smaller fullerenes as detailed in Ref. [22].

*Program Fullerene is an open-source code and is freely downloadable at http://ctcp.massey.ac.nz/index.php?page=fullerenes

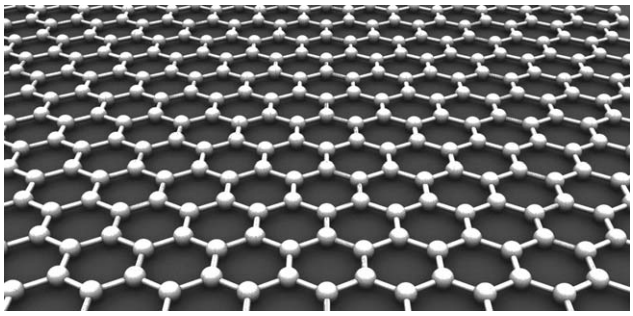

Figure 1. The structure of graphene.

The energy difference between C_{60} and graphene was calculated using the Vienna *Ab Initio* simulation package (VASP),[31] with a plane wave basis set (energy cutoff $E_c = 600$ eV) and a 1*s* frozen core PAW dataset.[32,33] Graphene sheets as shown in Figure 1, in the graphite arrangement, were kept 10 Å apart, and C_{60} was calculated in a cubic box of size 20 Å. All internal coordinates (and thus, the lattice constants of graphene) were optimized until residual forces were below 1 meV/Å. Here, we chose a variety of functionals as implemented in VASP,[31] namely the local density approximation (LDA), the PBE functional as already mentioned,[25] the PBE functional corrected using Grimme's dispersion correction (PBE-D2),[34,35] and the optB88-vdW functional Michaelides et al., and others.[36–38]

A General Harmonic Force Field for Fullerenes

The original program *Fullerene*[21] included a harmonic force field of the form

$$E_{\mathrm{HFF}} = \frac{k_\mathrm{p}}{2}\sum_{i_\mathrm{p}}^{\text{p-edges}}\left(R_{i_\mathrm{p}} - R_\mathrm{p}\right)^2 + \frac{k_\mathrm{h}}{2}\sum_{i_\mathrm{h}}^{\text{h-edges}}\left(R_{i_\mathrm{h}} - R_\mathrm{h}\right)^2 + \frac{f_\mathrm{p}}{2}\sum_{j_\mathrm{p}}^{60}\left(\alpha_{j_\mathrm{p}} - \alpha_\mathrm{p}\right)^2 + \frac{f_\mathrm{h}}{2}\sum_{j_\mathrm{h}}^{3N-60}\left(\alpha_{j_\mathrm{h}} - \alpha_\mathrm{h}\right)^2, \quad (1)$$

In this simple force field, introduced by Wu et al. for C_{60}-I_h,[12] bonded pairs of vertices are taken into account. k_p and k_h are the force constants for the two different C—C bonds (set to $\approx$ 300 kcal Å^{-2}), R_p and R_h the corresponding pentagon and hexagon bond distances ($\approx$1.4 Å), f_p and f_h are the force constants for the two different bending modes in a pentagon and hexagon with the corresponding bond angles α_p and α_h of

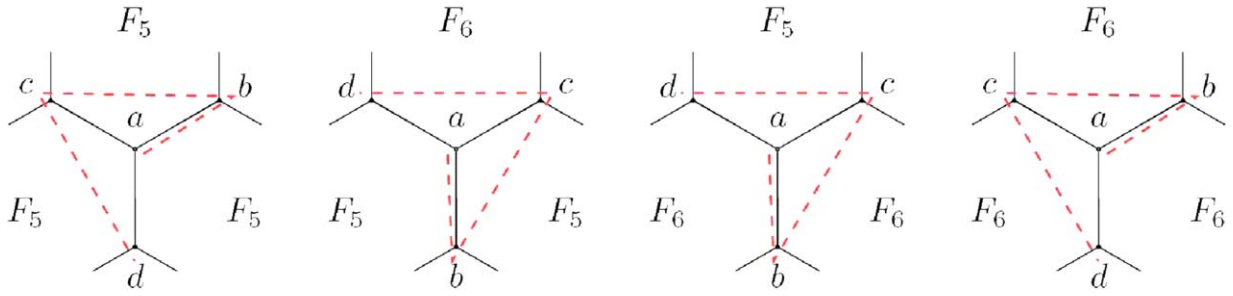

Figure 2. Unique and symmetry preserving layout of the four types of dihedral angles θ_{abcd}, depending on the adjacent faces. [Color figure can be viewed in the online issue, which is available at wileyonlinelibrary.com.]

108° and 120°, respectively. As the original Wu force field was developed for C_{60}-I_h only, bonds adjacent to two pentagons were treated in the same way as bonds adjacent to one pentagon and one hexagon in the program *Fullerene*.[21] The geometry can then be optimized using for example a Fletcher–Reeves–Polak–Ribiere geometry optimization with analytical gradients,[39] which is very computer time efficient even for larger fullerenes containing thousands of carbon atoms.[21,40]

The Wu force field is in principle applicable to all fullerenes and usually yields structures that are in good agreement with optimized structures from a more rigorous quantum theoretical treatment such as DFT. The root mean square (rms) deviations between DFT and force field optimized bond lengths are usually smaller than 0.05 Å.[21] However, the Wu force field suffers from two problems. First, the optimization may converge to local minima, especially if the initial structure is far from the real one. This may result in distortions away from convexity (dents) or, in the worst case, partially inverted structures with self-intersecting planes. Second, as no dihedral angles are restrained in this force field, the minimum geometry does not correctly reproduce the convexity or planarity of calculated geometries at DFT level of theory.

The former problem can be alleviated by adding a Coulomb repulsive potential in the initial phase of the geometry optimization,[21]

$$E = E_{\mathrm{HFF}} + E_{\mathrm{Coulomb}} = E_{\mathrm{HFF}} + \sum_{i=1}^{N} \frac{f_{\mathrm{Coulomb}}}{|\vec{r_i} - \vec{r_0}|} \tag{2}$$

with $\vec{r_i} - \vec{r_0}$ being the distance between vertex *i* and the barycenter at $\vec{r_0}$. f_{Coulomb} can be chosen as large as necessary to keep the fullerene cage in the right shape. Another more robust as well as more challenging solution to this issue is, to come up with an initial structure that is closer to the global minimum, for example, by directly deriving the shape of the ideal embedding from the graph.

As a solution to the second problem, we add a dihedral angle term to the Wu force field (the result is denoted as extended harmonic force field in the following, EHFF), which enhances planarity in areas of connected hexagons and enforces convexity in areas of positive Gaussian curvature. In addition to improving the global minimum structure, the dihedral angle term makes the force field more robust with respect to converging to the global minimum.

The extended Wu force field takes three types of bonds (in the ring fusion of 0, 1, or 2 pentagons), two types of angles, and four types of dihedral angles into account. There is one dihedral per atom that is uniquely defined with respect to the three adjacent faces (Fig. 2). Dihedrals θ_{abcd} are defined between one atom *a* and its three neighbors *b, c,* and *d*. Note that the connection *a–b* represents an edge in the graph, while *b–c* and *c–d* do not. As one atom is part of three faces (0, 1, 2, or 3 pentagons) there are four different types of dihedrals which differ in their respective zero value and force constant as shown in Figure 2. In the case of mixed adjacent faces, that is, vertex *a* being adjacent to one or two pentagons, vertex *b* is chosen to lie between the two equal faces, a choice that is unique and symmetry preserving. Vertices *c* and *d* are placed counter clockwise which leads to positive dihedral angles at convex vertices. This definition requires the least possible number of angle evaluations per vertex compared with for example the usual definition of a torsional motion.

The total energy for the EHFF force field is given by

$$\begin{aligned} E_{\mathrm{EHFF}} = {} & \frac{f_{\mathrm{pp}}}{2}\sum_{i_{\mathrm{pp}}}^{\mathrm{pp\text{-}e}}\left(R_{i_{\mathrm{pp}}} - R_{\mathrm{pp}}\right)^2 + \frac{f_{\mathrm{hp}}}{2}\sum_{i_{\mathrm{hp}}}^{\mathrm{hp\text{-}e}}\left(R_{i_{\mathrm{hp}}} - R_{\mathrm{hp}}\right)^2 + \frac{f_{\mathrm{hh}}}{2}\sum_{i_{\mathrm{hh}}}^{\mathrm{hh\text{-}e}}\left(R_{i_{\mathrm{hh}}} - R_{\mathrm{hh}}\right)^2 \\ & + \frac{f_{\mathrm{p}}}{2}\sum_{j_{\mathrm{p}}}^{60}\left(\alpha_{j_{\mathrm{p}}} - \alpha_{\mathrm{p}}\right)^2 + \frac{f_{\mathrm{h}}}{2}\sum_{j_{\mathrm{h}}}^{3N-60}\left(\alpha_{j_{\mathrm{h}}} - \alpha_{\mathrm{h}}\right)^2 + \frac{f_{\mathrm{ppp}}}{2}\sum_{k_{\mathrm{ppp}}}^{\mathrm{ppp\text{-}v}}\left(\theta_{k_{\mathrm{ppp}}} - \theta_{\mathrm{ppp}}\right)^2 \\ & + \frac{f_{\mathrm{hpp}}}{2}\sum_{k_{\mathrm{hpp}}}^{\mathrm{hpp\text{-}v}}\left(\theta_{k_{\mathrm{hpp}}} - \theta_{\mathrm{hpp}}\right)^2 + \frac{f_{\mathrm{hhp}}}{2}\sum_{k_{\mathrm{hhp}}}^{\mathrm{hhp\text{-}v}}\left(\theta_{k_{\mathrm{hhp}}} - \theta_{\mathrm{hhp}}\right)^2 + \frac{f_{\mathrm{hhh}}}{2}\sum_{k_{\mathrm{hhh}}}^{\mathrm{hhh\text{-}v}}\left(\theta_{k_{\mathrm{hhh}}} - \theta_{\mathrm{hhh}}\right)^2 \end{aligned} \tag{3}$$

where pp-e (hp-e, hh-e) denotes the number of edges adjacent to 2 (1, 0) pentagons, and ppp-v (hpp-v, hhp-v, hhh-v) is the number of vertices adjacent to 3 (2, 1, 0) pentagons. If required, the Coulomb repulsive potential in eq. (2) can be added to this force field for the initial geometry optimization.

The force-field parameters are set as follows: $R_{\mathrm{hp}} = 1.458$ Å and $R_{\mathrm{hh}} = 1.401$ Å are taken from an electron gas diffraction study of C_{60},[41] which are close to the distances obtained from X-ray diffraction measurements of solid C_{60} ($R_{\mathrm{hp}} = 1.455$ Å and $R_{\mathrm{hh}} = 1.391$ Å).[42] $R_{\mathrm{pp}} = 1.479$ Å has been estimated from PBE calculations on C_{50} and scaled with the experimental R_{hp} and R_{hh} for C_{60}. The angles in pentagons and hexagons have been set to $\alpha_{\mathrm{p}} = 108°$ and $\alpha_{\mathrm{h}} = 120°$ under the assumption that faces are planar. The dihedral angles $\theta_{\mathrm{ppp}} = 37.38°$, $\theta_{\mathrm{hpp}} = 29.20°$, $\theta_{\mathrm{hpp}} = 23.49°$, and $\theta_{\mathrm{hhh}} = 0.0°$ have been

Table 1. Properties of selected fullerenes C_N (N=20+2n, n∈$N_0\backslash\{1\}$) up to C_{60} (numbering of the isomers stems from lexicographically ordered face-spiral pentagon indices, see Ref. [3]) from the EHFF and DFT (PBE) optimizations using a def2-TZVPP basis set for carbon.

N	Isomer	IPG	R_{min}^{PBE}	R_{min}^{EHFF}	R_{max}^{PBE}	R_{max}^{EHFF}	ΔR_{rms}	$\Delta\alpha_{rms}$	$\Delta\theta_{rms}$	A^{PBE}	A^{EHFF}	ΔE_{RFS}^{PBE}	ΔE_{ZPV}^{EHFF}
20	1	I_h	1.409	1.479	1.514	1.479	0.041	1.63	1.88	43.64	45.16	18.148	0.13977
24	1	D_{6d}	1.373	1.460	1.530	1.481	0.054	1.28	1.91	54.66	55.82	15.710	0.14736
26	1	D_{3h}	1.384	1.458	1.540	1.484	0.047	1.69	1.95	59.88	61.24	14.024	0.15020
28	2	T_d	1.430	1.458	1.510	1.482	0.026	1.05	1.57	65.01	66.69	11.735	0.15261
30	3	C_{2v}	1.368	1.406	1.524	1.485	0.034	1.86	3.04	70.16	71.77	10.350	0.15472
32	6	D_3	1.384	1.406	1.503	1.482	0.036	1.48	2.69	75.37	77.08	8.369	0.15654
34	5	C_2	1.389	1.403	1.503	1.483	0.033	1.62	2.67	80.66	82.21	8.029	0.15810
36	15	D_{6h}	1.414	1.401	1.490	1.479	0.030	0.70	1.27	85.87	87.55	7.126	0.15949
38	17	C_2	1.377	1.401	1.491	1.481	0.034	1.25	2.20	91.31	92.71	6.409	0.16072
40	38	D_2	1.377	1.402	1.497	1.480	0.034	1.46	2.61	96.67	97.90	5.749	0.16184
42	45	D_3	1.383	1.402	1.489	1.481	0.030	1.49	2.39	101.8	103.1	5.012	0.16284
44	75	D_2	1.384	1.401	1.481	1.480	0.027	1.36	2.21	107.1	108.3	4.296	0.16368
46	109	C_2	1.395	1.398	1.483	1.481	0.030	1.64	4.30	112.4	113.2	4.066	0.16522
48	171	C_2	1.387	1.399	1.480	1.479	0.027	1.65	4.28	117.6	118.3	3.384	0.16587
50	271	D_{5h}	1.395	1.401	1.468	1.474	0.021	1.01	1.71	122.8	123.9	2.526	0.16591
52	422	C_2	1.389	1.399	1.480	1.479	0.031	1.94	5.57	128.2	128.5	2.512	0.16782
54	540	C_{2v}	1.379	1.398	1.480	1.479	0.024	1.19	3.80	133.4	134.0	1.921	0.16766
56	916	D_2	1.382	1.396	1.469	1.477	0.026	1.54	4.70	138.8	139.0	1.560	0.16877
58	1205	C_{3v}	1.391	1.397	1.467	1.479	0.022	1.48	4.65	144.0	144.2	1.260	0.16911
60	1812	I_h	1.399	1.401	1.452	1.458	0.005	0.06	0.02	149.1	150.1	0.000	0.16851

Ideal point group symmetry IPG, smallest R_{min} and largest R_{max} bond distances, rms between the force-field and PBE calculated distances ΔR_{rms}, bond angles $\Delta\alpha_{rms}$ and torsions between adjacent carbon atoms $\Delta\theta_{rms}$ (for the torsions a positive value implies a convex arrangement), surface area A in Å^2, the PBE total energy ΔE_{RFS}^{PBE} per carbon atom relative to C_{60} in kcal/mol, and the force-field zero-point vibrational energy contribution ΔE_{ZPV}^{EHFF} per carbon atom in eV.

calculated assuming planar faces and the above given bond lengths. It is clear that for many fullerenes the optimized structural parameters can deviate substantially from the ideal ones given in this force field, for example, two neighboring hexagons in carbon nanotubes are not in one plane. Nevertheless, the structures we obtain are rather accurate as we shall see.

From the least squares fit to B3LYP frequencies of the vibrational spectra of C_{50}-C_1(193), C_{60}-I_h(1812) and C_{70}-D_{5h}(8149) (numbering of the isomers stems from lexicographically ordered face-spiral pentagon indices, see Ref. [3]), we obtain the following force constants for the force field shown in eq. (3) (in N/m or Nm/deg[2]): $f_{pp}=260.0, f_{hp}=390.0, f_{hh}=450.0, f_p=100.0, f_h=100.0, f_{ppp}=35.0, f_{pph}=65.0, f_{phh}=85.0, f_{hhh}=270.0$. The stretching and bending force constants are not too far away from the original force-field parameters published by Wu et al.[12] or Ceulemans et al.[16] Within the extended force field, frequencies are obtained through analytical second derivatives. The (rms) deviation of the fit $\Delta\omega_{rms}=45.5$ cm^{-1} is relatively small considering the fact that such a simple force field does not correctly describe the coupling between the stretching, bending, and torsional modes in terms of the correct normal modes.

Results and Discussion

The results of our EHFF and PBE calculations are shown in Tables 1 and 2. Here, we only give the ideal point group of the graph, which is reproduced by the force field, even though a DFT geometry optimization may reduce the symmetry due to Jahn–Teller distortions (see for example the discussion in Refs. [9,22]). The rms deviations listed for the bond lengths, bond angles, and torsion angles show that the EHFF performs well, especially if we consider that the bond lengths have been fixed to experimental values (note that the rms error for the bond distances can be considerably reduced if we use distances closer to the PBE optimized structure). The rms error is therefore predominantly caused by the fact that the DFT optimized structures have bond lengths with larger spreads. The smallest deviation is observed for C_{60} as we expect from the near ideal spherical geometry of this molecule. Moreover, if we compare the zero-point vibrational energy, which we obtained at the B3LYP level of theory for C_{50}-C_1(193) with 0.1667 eV/atom (this isomer is not listed in Table 1), C_{60}-I_h(1812) with 0.1705 eV/atom, and C_{70}-D_{5h}(8149) with 0.1711 eV/atom, we see that these are in excellent agreement with the values obtained from the general force field with 0.1681 eV/atom, 0.1685 eV/atom, and 0.1726 eV/atom, respectively. The force field structures of the two largest isolated pentagon rule (IPR) fullerenes C_{980}-I_h and C_{980}-I are shown in Figure 3 in comparison with the PBE optimized structures. It is not easy to spot differences between the two structures with the naked eye, except perhaps for the curvature around the pentagons. We conclude that our force-field optimized structures, which are computationally very efficient, are ideal to be used as starting geometries for a more elaborate quantum theoretical treatment.

Tables 1 and 2 also show the stability of the fullerenes with respect to C_{60} according to the isodesmic reaction $1/60\ E(C_{60}) \rightarrow 1/N\ E(C_N)$ (relative fullerene stability, RFS),

Table 2. Properties of selected fullerenes C_N for $N \geq 60$ (numbering of the isomers stems from lexicographically ordered face-spiral pentagon indices up to C_{100}, see Ref. [3], otherwise the Goldberg–Coxeter symbols (*k*, *l*) are given) from the EHFF and DFT (PBE/def2-SVP) optimizations.

N	Isomer	IPG	R_{min}^{PBE}	R_{min}^{EHFF}	R_{max}^{PBE}	R_{max}^{EHFF}	ΔR_{rms}	$\Delta\alpha_{rms}$	$\Delta\theta_{rms}$	A^{PBE}	A^{EHFF}	ΔE_{RFS}^{PBE}	ΔE_{ZPV}^{EHFF}
60	1812	I_h	1.407	1.401	1.457	1.458	0.004	0.06	0.03	150.3	150.1	0.000	0.16851
70	8149	D_{5h}	1.402	1.395	1.474	1.461	0.022	2.06	6.38	177.1	174.9	−0.875	0.17262
72	11190	D_{6d}	1.390	1.395	1.470	1.468	0.029	1.69	5.23	182.5	179.8	−0.476	0.17341
74	14246	D_{3h}	1.397	1.397	1.476	1.463	0.026	2.20	7.30	187.9	184.8	−0.913	0.17394
76	19150	D_2	1.395	1.392	1.476	1.466	0.029	2.37	6.95	193.2	189.8	−1.039	0.17456
76	19151	T_d	1.396	1.398	1.477	1.461	0.028	2.28	7.84	193.3	189.8	−0.900	0.17453
78	24105	D_3	1.393	1.392	1.474	1.463	0.032	2.51	7.01	198.5	194.8	−1.222	0.17512
78	24107	C_{2v}	1.385	1.397	1.476	1.464	0.029	2.53	7.88	198.6	194.8	−1.087	0.17509
78	24108	D_{3h}	1.369	1.396	1.472	1.464	0.033	2.26	6.43	198.6	194.7	−1.175	0.17521
78	24109	D_{3h}	1.382	1.398	1.474	1.461	0.029	2.47	8.35	198.6	194.8	−0.897	0.17511
80	31924	I_h	1.424	1.401	1.458	1.457	0.027	2.35	8.80	204.0	199.7	−0.979	0.17562
92	126409	T	1.387	1.395	1.474	1.460	0.037	2.94	8.72	236.1	229.7	−1.681	0.17841
100	285880	C_{2v}	1.376	1.370	1.474	1.468	0.041	3.24	8.08	257.3	249.9	−2.121	0.17991
140	(2, 1)	I	1.404	1.387	1.461	1.467	0.046	4.31	8.62	364.0	351.0	−3.770	0.18432
180	(3, 0)	I_h	1.401	1.373	1.457	1.473	0.050	3.89	6.72	470.7	452.8	−4.708	0.18686
240	(2, 2)	I_h	1.399	1.385	1.452	1.473	0.045	3.64	5.75	630.2	605.3	−5.577	0.18895
260	(3, 1)	I	1.402	1.384	1.459	1.474	0.045	3.31	5.12	683.5	656.3	−5.475	0.18951
320	(4, 0)	I_h	1.399	1.385	1.455	1.474	0.043	2.78	4.40	843.1	809.2	−5.964	0.19060
380	(3, 2)	I	1.399	1.387	1.454	1.472	0.041	2.59	4.12	1002.7	961.9	−6.356	0.19131
420	(4, 1)	I	1.400	1.388	1.448	1.472	0.039	2.35	3.89	1109.0	1063.9	−6.594	0.19177
500	(5, 0)	I_h	1.401	1.387	1.447	1.471	0.038	2.07	3.62	1324.4	1267.7	−6.800	0.19238
540	(3, 3)	I_h	1.400	1.386	1.445	1.470	0.037	2.01	3.52	1428.3	1369.5	−7.019	0.19263
560	(4, 2)	I	1.401	1.387	1.445	1.470	0.037	1.96	3.45	1481.5	1420.5	−7.002	0.19271
620	(5, 1)	I	1.401	1.387	1.445	1.469	0.036	1.83	3.35	1641.2	1573.4	−7.152	0.19305
720	(6, 0)	I_h	1.401	1.386	1.441	1.469	0.035	1.70	3.16	1907.1	1828.2	−7.386	0.19341
740	(4, 3)	I	1.401	1.385	1.444	1.469	0.035	1.68	3.09	1960.4	1879.1	−7.397	0.19346
780	(5, 2)	I	1.401	1.385	1.441	1.469	0.035	1.64	3.04	2066.8	1981.0	−7.489	0.19359
860	(6, 1)	I	1.402	1.384	1.443	1.468	0.035	1.55	2.93	2279.7	2184.9	−7.764	0.19382
960	(4, 4)	I_h	1.401	1.383	1.440	1.468	0.034	1.49	2.77	2545.7	2439.8	−7.718	0.19401
980	(5, 3)	I	1.402	1.383	1.443	1.469	0.033	1.48	2.75	2599.0	2490.7	−7.712	0.19405
980	(7, 0)	I_h	1.401	1.383	1.442	1.468	0.034	1.47	2.77	2599.0	2490.7	−7.709	0.19405
∞	–	–	1.425	1.401	1.425	1.401	0.024	0	0	–	–	−8.863[a]	0.196[b]

[a] See Table 3 for graphene data. [b] The ZPV energy contribution of graphene is the extrapolated value from the fullerene data. Ideal point group symmetry IPG, smallest R_{min} and largest R_{max} bond distances, rms error between the force-field and PBE calculated distances ΔR_{rms}, bond angles $\Delta\alpha_{rms}$ and torsions between adjacent carbon atoms $\Delta\theta_{rms}$ (for the torsions a positive value implies a convex arrangement), surface area *A* in Å^2, the PBE total energy ΔE_{RFS}^{PBE} per carbon atom relative to C_{60} in kcal/mol, and the force-field zero-point vibrational energy contribution ΔE_{ZPV}^{EHFF} per carbon atom in eV.

$$\Delta E_{RFS}(N) = 1/60\ E(C_{60}) - 1/N\ E(C_N) \quad (4)$$

where $E(C_N)$ is the total electronic energy obtained from the DFT calculation. Figure 4 compares the different RFS energies. It is clear that for $N \to \infty$, we approach the graphene limit as the size of planar hexagon sheets increase and the pentagons become less relevant in this limit. An extrapolation to $N \to \infty$ using all fullerenes shown in Tables 1 and 2 and a N^{-1} law for $\Delta E_{RFS}(N)$ (NB: the N^{-1} law comes from the curvature term or strain energy in fullerenes, for details see Refs. [19,43–46]),[9] gives −8.06 kcal/mol at the PBE level of theory (and −8.42 kcal/mol at the B3LYP level of theory). However, the $\Delta E_{RFS}(N)$ behavior is not strictly linear with N^{-1}. A linear extrapolation for the $\Delta E_{RFS}(N)$ values using larger fullerenes with $N \geq 500$ gives $\Delta E_{RFS} = -8.64$ kcal/mol at the PBE level of theory (−9.22 kcal/mol at the B3LYP level of theory) in much better agreement with the periodic boundary calculations listed in Table 3. More importantly, Figure 4 supports Schleyer's hypothesis that fullerenes are not highly stable molecules,[6] there is no "magic" stability of C_{60} compared with all the other fullerenes and especially graphene.

The graph representing C_{60} has 90 edges, out of these only one-third are double bonds (giving rise to 12,500 Kekulé structures of which 158 are symmetry distinct).[47–49] Moreover, the heat of formation cannot be simply derived from single and double bond energy increments as there is an additional repulsive curvature term from the 12 pentagons in the fullerene, which is mainly responsible for the difference in stability to graphene.[50] However, this curvature term approaches zero as "spherical" fullerenes with pentagons separated as far as possible from each other grow toward infinity ($N \to \infty$). Such fullerenes can be obtained as Goldberg–Coxeter transformations of C_{20}, that is, $GC_{k,l}[C_{20}]$. This is the main reason why we used this class of fullerenes (up to C_{980}) to obtain the graphene limit. For a recent interesting discussion on smooth scaling of fullerene properties toward the graphene limit see Lewis et al.[51]

In a recent paper by Radom and coworkers, the heat of formation for C_{60} was calculated accurately to be 602.7 kcal/mol,[52] which translates into 10.0 kcal/mol per carbon atom. This value is already in very good agreement with our PBE or B3LYP graphene limit value (mean value between both levels

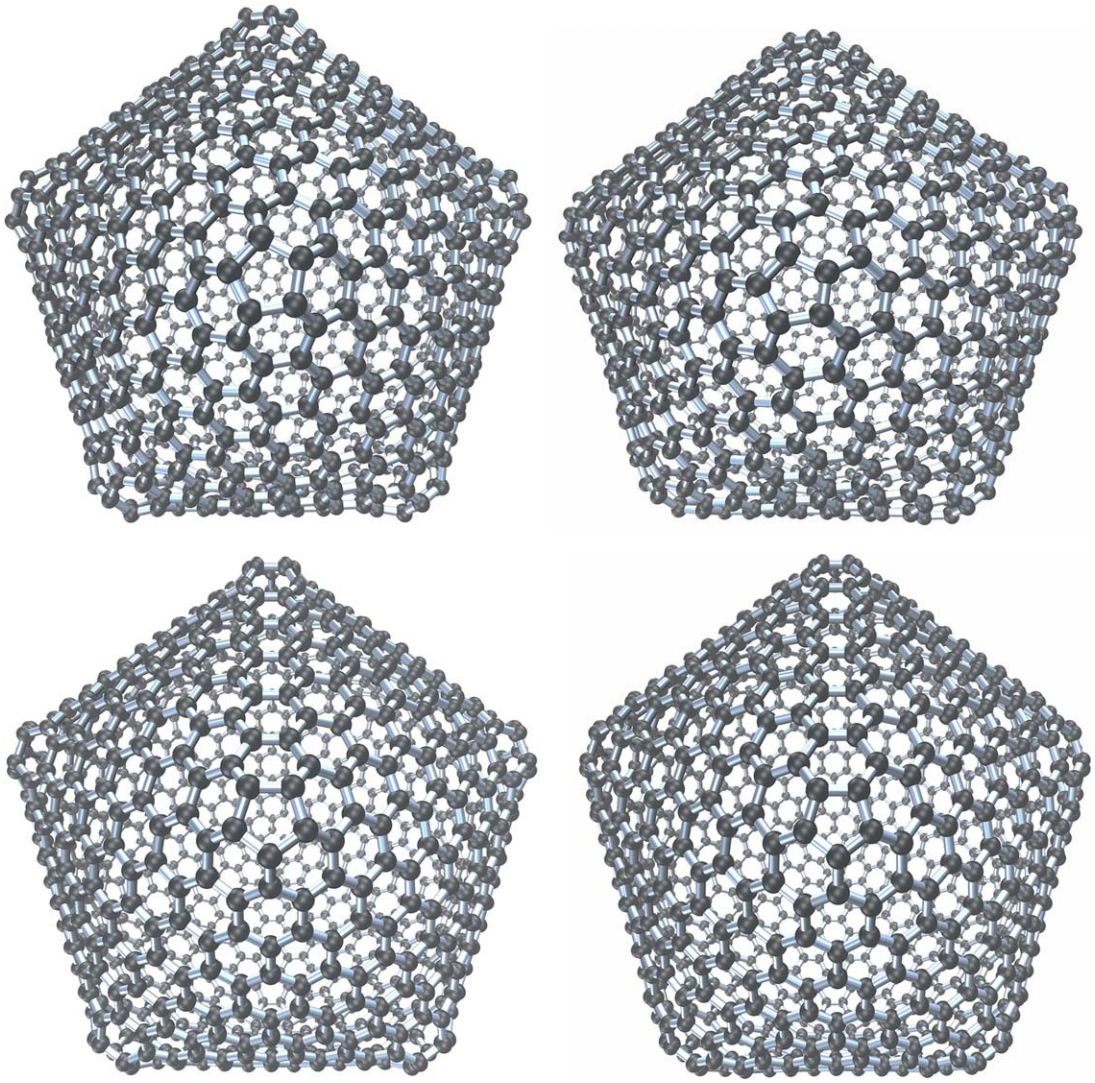

Figure 3. Force-field (left) and PBE optimized (right) structures of C_{980}-*I* (top) and C_{980}-I_h (bottom). [Color figure can be viewed in the online issue, which is available at wileyonlinelibrary.com.]

of theory is 8.9 ± 0.3 kcal/mol which is in the range of values listed in Table 3). Taking into account the small Van der Waals interactions between the graphene sheets in graphite (+1.5 kcal/mol)[53] and differences in zero-point vibrational energy between C_{60} and graphene (−0.63 kcal/mol, see discussion below), and neglecting finite temperature effects, we arrive at a heat of formation for C_{60} of 596 ± 20 kcal/mol in excellent agreement with the value by Radom and coworkers or with the NIST recommended value of 612 ± 24 kcal/mol.[54,55] Note that already in 1996 Dunlap and Boettger discussed the graphene limit for fullerenes by LDA calculations.[19] In another study, Dunlap and Zope obtained an enthalpy of formation of 594 kcal/mol for C_{60} using an Xα approximation (with an α-value of 0.64190).[20]

Turning to the zero-point vibrational energy ΔE_{ZPV}, which we obtain from our force-field calculations, we see from Figure 5 that for the larger IPR fullerenes, ΔE_{ZPV}^{EHFF} follows an almost perfect linear trend with respect to N^{-1} for C_{60} onwards. In fact, the fullerenes with adjacent pentagons also follow a linear trend, but different to the isolated pentagon fullerenes. From the latter we can extrapolate the harmonic zero-point vibrational energy contribution for graphene as 0.196 eV per carbon atom. This value should be rather accurate as the

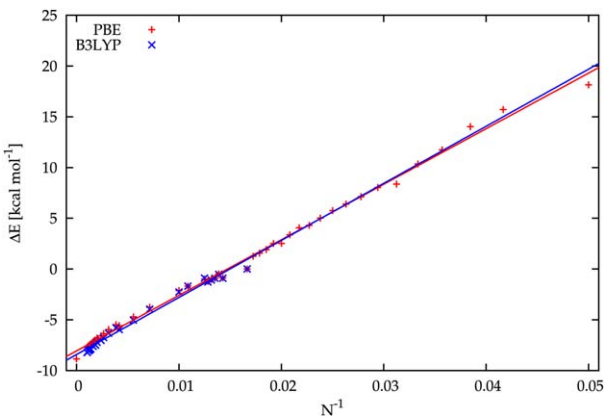

Figure 4. ΔE_{RFS}^{PBE} for the fullerenes as listed in Tables 1 and 2 plotted against N^{-1}. For the PBE functional the graphene limit is shown (see Table 3), and for C_{60} onwards B3LYP results are also shown.

Table 3. C—C bond distance R_{CC} (in Å), total energies E_T (in eV/atom) for graphene (G) and C_{60}, calculated in a plane wave implementation of various DFT functionals, and the energy difference $\Delta E(\infty)$ (in kcal/mol) between the different allotropes ($C_{60} \rightarrow$ graphene, per atom).

DFT method	R_{CC}	E_T(G)	$E_T(C_{60})$	$\Delta E(\infty)$
LDA	1.413	−10.0917	−9.7074	−8.862
PBE	1.425	−9.2271	−8.8530	−8.627
PBE-D2	1.425	−9.2821	−8.9051	−8.694
optB88-vdW	1.423	−7.9515	−7.5702	−8.793
exp.	1.42	–	–	–

ΔE_{ZPV}^{EHFF} values for C_{50}, C_{60}, and C_{70} were in good agreement with the PBE results as already discussed. This value is of the right order and can also be deduced from calculated phonon dispersion curves and experimental Raman frequencies for graphene.[56] Even though the phonon dispersion curves are known rather accurately,[56–58] we only found one publication using a semiempirical approach for the zero-point vibrational energy including anharmonicity effects, which gave a value of 0.165 eV per carbon atom somewhat below our extrapolated value.[59] Another value (0.181 eV) comes from PBE calculations of graphite,[60] which should be close to the graphene value.

Summary and Conclusions

We have implemented a general force field as part of the program *Fullerene*,[21] which works for all fullerenes. Structure optimizations show that geometries obtained from this force field are in excellent agreement with those obtained from DFT. This force field is easily extendable to more general polyhedral structures. Isodesmic reaction energies ΔE_{RFS} compared with C_{60}-I_h for Goldberg–Coxeter fullerenes were used to extrapolate to the graphene limit. The extrapolated ΔE_{RFS} graphene value was used to obtain the heat of formation of C_{60}, which is in very good agreement with the more accurate value published by Radom and coworkers.[52] The force constants of the general force field were adjusted to the vibrational spectrum of three selected fullerenes, which gives rather accurate values for the zero-point vibrational contribution ΔE_{ZPV}^{EHFF}. Extrapolation to the graphene limit allows to obtain the ΔE_{ZPV}^{EHFF} value for graphene, which is in reasonable agreement with estimates from phonon dispersion calculations.

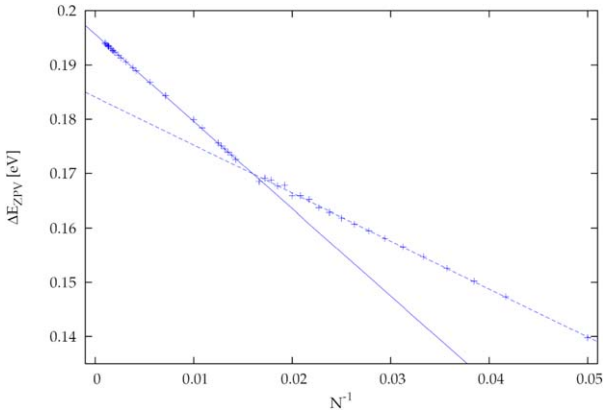

Figure 5. ΔE_{ZPV}^{EHFF} for the fullerenes as listed in Tables 1 and 2 plotted against N^{-1}. For the linear fit the data are split in two regions, $N \geq 60$ (solid line) and $N \leq 60$ (dashed line).

Acknowledgments

R.T. thanks the LOEWE-CSC, H.L.R. Stuttgart, and H.R.Z. Marburg for computational resources and the AvH (Bonn) for support via an alumni fellowship. The authors thank James Avery (Copenhagen) for valuable discussions and Stefan Grimme (Bonn) for his support.

Keywords: fullerenes · graphene · force field · density functional theory

How to cite this article: L. N. Wirz, R. Tonner, A. Hermann, R. Sure, P. Schwerdtfeger. *J. Comput. Chem.* **2016**, *37*, 10–17. DOI: 10.1002/jcc.23894

Additional Supporting Information may be found in the online version of this article.

[1] H. W. Kroto, J. R. Heath, S. C. O'Brien, R. F. Curl, R. E. Smalley, *Nature* **1985**, *318*, 162.
[2] H. Kroto, *Angew. Chem. Int. Ed.* **1997**, *36*, 1578.
[3] P. W. Fowler, D. E. Manolopoulos, An Atlas of Fullerenes, 2nd ed.; Dover Publications: Mineola, New York, **2006**.
[4] F. Cataldo, A. Graovac, O. Ori, The Mathematics and Topology of Fullerenes; Springer: Berlin, **2011**.
[5] A. Hirsch, Z. Ruoff, H. Jiao, *Angew. Chem. Int. Ed.* **2000**, *39*, 3915.
[6] Z. Chen, J. I. Wu, C. Corminboeuf, J. Bohmann, X. Lu, A. Hirsch, P. V. R. Schleyer, *Phys. Chem. Chem. Phys.* **2012**, *14*, 14886.
[7] M. Garcia-Borr'as, S. Osuna, J. M. Luis, M. Swart, M. Sol'a, *Chem. Soc. Rev.* **2014**, *43*, 5089.
[8] W. P. Thurston, Geometry & Topology Monographs, the Epstein Birthday Schrift, **1998**.
[9] P. Schwerdtfeger, L. N. Wirz, J. Avery, *WIREs Comput. Mol. Sci.* **2015**, *5*, 96.
[10] D. E. Manolopoulos, P. W. Fowler, *J. Chem. Phys.* **1992**, *96*, 7603.
[11] W. T. Tutte, *Proc. Lond. Math. Soc.* **1963**, *13*, 743.
[12] Z. Wu, D. A. Jelski, T. F. George, *Chem. Phys. Lett.* **1987**, *137*, 291.
[13] S. J. Cyvin, E. Brendsdal, B. N. Cyvin, J. Brunvoll, *Chem. Phys. Lett.* **1988**, *143*, 377.
[14] R. A. Jishi, R. M. Mirie, M. S. Dresselhaus, *Phys. Rev. B* **1992**, *45*, 13685.
[15] J. L. Feldman, J. Q. Broughton, L. L. Boyer, D. E. Reich, M. D. Kluge, *Phys. Rev. B* **1992**, *46*, 12731.
[16] A. Ceulemans, P. W. Fowler, I. Vos, *J. Chem. Phys.* **1994**, *100*, 5491.
[17] A. Ceulemans, B. C. Titeca, L. F. Chibotaru, I. Vos, P. W. Fowler, *J. Phys. Chem. A* **2001**, *105*, 8284.
[18] I. D. Hands, J. L. Dunn, C. A. Bates, *J. Chem. Phys.* **2004**, *120*, 6912.
[19] B. I. Dunlap, J. C. Boettger, *J. Phys. B At. Mol. Opt. Phys.* **1996**, *29*, 4907.
[20] B. I. Dunlap, R. R. Zope, *Chem. Phys. Lett.* **2006**, *422*, 451.
[21] P. Schwerdtfeger, L. Wirz, J. Avery, *J. Comput. Chem.* **2013**, *34*, 1508.
[22] R. Sure, R. Tonner, P. Schwerdtfeger, *J. Comput. Chem.* **2015**, *36*, 88.
[23] M. Goldberg, *Tohoku Math. J.* **1937**, *43*, 104.
[24] H. S. M. Coxeter, In A Spectrum of mathematics - Essays Presented to H. G. Forder, J. C. Butcher, ed.; Oxford University press, Oxford, **1971**; pp. 98–107.
[25] J. P. Perdew, K. Burke, M. Ernzerhof, *Phys. Rev. Lett.* **1996**, *77*, 3865.
[26] F. Weigend, R. Ahlrichs, *Phys. Chem. Chem. Phys. 7*, 2005, 3297.
[27] M. J. Frisch, G. W. Trucks, H. B. Schlegel, G. E. Scuseria, M. A. Robb, J. R. Cheeseman, G. Scalmani, V. Barone, B. Mennucci, G. A. Petersson, H. Nakatsuji, M. Caricato, X. Li, H. P. Hratchian, A. F. Izmaylov, J. Bloino, G.

Zheng, J. L. Sonnenberg, M. Hada, M. Ehara, K. Toyota, R. Fukuda, J. Hasegawa, M. Ishida, T. Nakajima, Y. Honda, O. Kitao, H. Nakai, T. Vreven, J. A. Montgomery, Jr., J. E. Peralta, F. Ogliaro, M. Bearpark, J. J. Heyd, E. Brothers, K. N. Kudin, V. N. Staroverov, R. Kobayashi, J. Normand, K. Raghavachari, A. Rendell, J. C. Burant, S. S. Iyengar, J. Tomasi, M. Cossi, N. Rega, J. M. Millam, M. Klene, J. E. Knox, J. B. Cross, V. Bakken, C. Adamo, J. Jaramillo, R. Gomperts, R. E. Stratmann, O. Yazyev, A. J. Austin, R. Cammi, C. Pomelli, J. W. Ochterski, R. L. Martin, K. Morokuma, V. G. Zakrzewski, G. A. Voth, P. Salvador, J. J. Dannenberg, S. Dapprich, A. D. Daniels, Ö. Farkas, J. B. Foresman, J. V. Ortiz, J. Cioslowski, D. J. Fox, *Gaussian Inc: Wallingford CT* **2009**.

[28] A. D. Becke, *J. Chem. Phys.* **1993**, *98*, 5648.

[29] C. Lee, W. Yang, R. G. Parr, *Phys. Rev. B* **1988**, *37*, 785.

[30] R. Ahlrichs, M. K. Armbruster, M. Bär, R. B. H.-P. Baron, N. Crawford, P. Deglmann, M. Ehrig, K. Eichkorn, S. Elliott, F. Furche, F. Haase, M. Häser, H. Horn, C.HättigC. Huber, U. Huniar, M. Kattannek, A. Köhn, C. Kölmel, M. Kollwitz, K. May, P. Nava, C. Ochsenfeld, H. Öhm, H. Patzelt, D. Rappoport, O. Rubner, A. Schäfer, U. Schneider, M. Sierka, O. Treutler, B. Unterreiner, M. von Arnim, F. Weigend, P. Weis, H. Weiss, program Turbomole, Version 6.3, Universität Karlsruhe **2012**. Available at http://www.turbomole.com.

[31] G. Kresse, J. Furthmüller, *Phys. Rev. B* **1996**, *54*, 11169.

[32] P. E. Blöchl, *Phys. Rev. B* **1994**, *50*, 17953.

[33] G. Kresse, D. Joubert, *Phys. Rev. B* **1999**, *59*, 1758.

[34] S. Grimme, *J. Comput. Chem.* **2006**, *27*, 1787.

[35] T. Risthaus, S. Grimme, *J. Chem. Theory Comput.* **2013**, *9*, 1580.

[36] M. Dion, H. Rydberg, E. Schröder, D. C. Langreth, B. I. Lundqvist, *Phys. Rev. Lett.* **2004**, *92*, 246401.

[37] J. Klimeš, D. R. Bowler, A. Michaelides, *J. Phys. Condens. Matter* **2010**, *22*, 022201.

[38] K. Lee, E. D. Murray, L. Kong, B. I. Lundqvist, D. C. Langreth, *Phys. Rev. B* **2010**, *82*, 081101.

[39] W. H. Press, Numerical Recipes 3rd edition: The Art of Scientific Computing, Cambridge University Press, Cambridge, **2007**.

[40] L. N. Wirz, J. E. Avery, P. Schwerdtfeger, *J. Chem. Inf. Model.* **2014**, *54*, 12114.

[41] K. Hedberg, L. Hedberg, D. S. Bethune, C. A. Brown, H. C. Dorn, R. D. Johnson, M. de Vries, *Science* **1991**, *254*, 410.

[42] W. I. F. David, R. M. Ibberson, J. C. Matthewman, K. Prassides, T. J. S. Dennis, J. P. Hare, H. W. Kroto, R. Taylor, D. R. M. Walton, *Nature* **1991**, *353*, 147.

[43] T. G. Schmalz, W. A. Seitz, D. J. Klein, G. E. Hite, *J. Am. Chem. Soc.* **1988**, *110*, 1113.

[44] D. Bakowies, W. Thiel, *J. Am. Chem. Soc.* **1991**, *113*, 3704.

[45] J. Cioslowski, N. Rao, D. Moncrieff, *J. Am. Chem. Soc.* **2000**, *122*, 8265.

[46] A. S. Barnard, S. P. Russo, I. K. Snook, *J. Comp. Phys.* **2003**, *118*, 5094.

[47] D. J. Klein, T. G. Schmalz, G. E. Hite, W. A. Seitz, *J. Am. Chem. Soc.* **1986**, *108*, 1301.

[48] D. Vukičević, H. W. Kroto, M. Randić, *Croat. Chem. Acta* **2005**, *78*, 223.

[49] M. Randić, H. W. Kroto, D. Vukičević, *J. Chem. Inf. Model.* **2007**, *47*, 897.

[50] J. Cioslowski, Electronic Structure Calculations on Fullerenes and Their Derivatives; Wooden Books: New York, **1995**.

[51] G. R. Lewis, W. E. Bunting, R. R. Zope, B. I. Dunlap, J. C. Ellenbogen, *Phys. Rev. A* **2013**, *87*, 052515.

[52] A. Karton, B. Chan, K. Raghavachari, L. Radom, *J. Phys. Chem. A* **2013**, *117*, 1834.

[53] Y. J. Dappe, M. A. Basanta, F. Flores, J. Ortega, *Phys. Rev. B* **2006**, *74*, 205434.

[54] H.-D. Beckhaus, S. Verevkin, C. Rüchardt, F. Diederich, C. Thilgen, H.-U. T. Meer, H. Mohn, W. Müller, *Angew. Chem.* **1994**, *33*, 996.

[55] H. Y. Afeefy, J. F. Liebman, S. E. Stein, Neutral Thermochemical Data. In NIST Chemistry WebBook, NIST Standard Reference Database, Number 69; P. J. Linstrom, W. G. Mallard, Eds.; National Institute of Standards and Technology: Gaithersburg, MD, **2006**. Available at http://webbook.nist.gov (accessed January 1, 2015).

[56] O. Dubay, G. Kresse, *Phys. Rev. B* **2003**, *67*, 035401.

[57] N. Mounet, N. Marzari, *Phys. Rev. B* **2005**, *71*, 205214.

[58] M. Lazzeri, C. Attaccalite, L. Wirtz, F. Mauri, *Phys. Rev. B* **2008**, *78*, 081406.

[59] I. L. Locht, The effect of temperature on the phonon dispersion relation in graphene, Master thesis, Radboud University of Nijmegen: Nijmegen, Netherlands, **2012**.

[60] W. Grochala, *Angew. Chem. Int. Ed.* **2014**, *53*, 3680.

Received: 10 February 2015
Revised: 17 February 2015
Accepted: 21 February 2015
Published online on 26 March 2015